Spec. Publs int. Ass. Sediment. (1998) **26**, 461–481

Application of quantitative back-scattered electron image analysis in isotope interpretation of siderite cement: Tirrawarra Sandstone, Cooper basin, Australia

M.R. REZAEE *and* J.P. SCHULZ-ROJAHN[1]

Australian Petroleum Cooperative Research Centre (APCRC), National Centre for Petroleum Geology and Geophysics (NCPGG), Thebarton Campus, University of Adelaide, SA 5005, Australia

ABSTRACT

A new method is presented to improve the interpretation of bulk-rock oxygen and carbon isotope data in isotopically heterogeneous samples. In the fluvio-deltaic Tirrawarra Sandstone of the Fly Lake and Moorari Fields, Cooper basin, Australia, volumetric estimation of individual cement generations of siderite is accomplished using image analysis techniques in conjunction with electron microprobe data. Results show that bulk-rock isotope values are controlled by the relative proportions of three main siderite cement generations. The variation in $\delta^{18}O$ can be expressed by the equation $\delta^{18}O_{(bulk)} = (V_{S1} \times \delta^{18}O_{S1}) + (V_{S2} \times \delta^{18}O_{S2}) + (V_{S3} \times \delta^{18}O_{S3})$. The variation in $\delta^{13}C$ can be expressed by the same type of equation, but the correlation coefficient is lower (0.64) than the one for $\delta^{18}O$ (0.82). The $\delta^{18}O$ and $\delta^{13}C$ end-member values for each cement generation are characterized by a narrow range, allowing a precise definition of the conditions under which individual generations formed. Integration of petrographic and fluid inclusion results has led to the identification of the following siderite cementation events: (i) an early, homogeneous Fe-rich siderite with a $\delta^{13}C$ signature of +1.45‰, indicative of low-temperature methanogenic processes (≤30°C); (ii) an Mg-rich inhomogeneous siderite characterized by a complex zoning, with a $\delta^{13}C$ signature of –8.5‰ produced mainly by the decarboxylation of organic matter at temperatures between 64 and 76°C; (iii) an Mg-rich, relatively homogeneous pore-filling siderite with a $\delta^{13}C$ character of –11‰ that was produced during kerogen maturation, at more elevated temperatures (98–110°C). Both the first and second generation of siderite cement were followed by a period of cement dissolution. The technique presented here has particular applications in cases where pure or nearly pure samples of end-member siderite cement generations are not available for isotope analysis, provided the various cement generations have different chemical compositions.

INTRODUCTION

Siderite can form in a wide variety of depositional and diagenetic environments, including in marine, brackish and fresh-water settings (e.g. Gould & Smith, 1979; Matsumoto & Iijima, 1981; Gautier, 1982; Curtis & Coleman, 1986; Carpenter *et al.*, 1988; Bahrig, 1989; Mozley, 1989; Mozley & Carothers, 1992; Spiro *et al.*, 1993; Morad *et al.*, 1994). The mineral is most suitable for the study of pore-water evolution during sediment subsidence because, unlike other carbonate minerals, siderite probably does not undergo recrystallization and isotope re-equilibration during burial diagenesis, as it has no unstable precursors or polymorphs (Curtis *et al.*, 1975; Gautier, 1982; Pearson, 1985; Curtis & Coleman, 1986). Therefore, stable isotope data of siderite cements can provide a powerful tool for the interpretation of diagenetic events in geological

[1]Present address: Shell Development (Australia) Pty Ltd, 1 Spring Street, Melbourne, Victoria 3000, Australia, e-mail jorg.p.schulzrojahn@shell.com.au, WWW http://www.ncpgg.adelaide.edu.au/jorg.htm

provinces. However, siderite rarely represents the only carbonate material in sedimentary rocks, and mechanical and/or chemical methods must be employed to separate the siderite from other carbonate minerals in order to obtain an isotopically homogeneous sample (see Al-Aasm *et al.*, 1990). However, even rocks containing only one carbonate cement type can be characterized by widely varying bulk isotope compositions in the same geological province. The bulk-rock isotope compositional variations for rocks with only one carbonate type can be caused by the presence of multiple carbonate cement generations which cannot be chemically separated from each other for separate isotope analysis. In recent years, advancements in laser ablation and ion microprobe technology have led to improvements in spatially resolved isotope analysis (e.g. Dickson *et al.*, 1990; Smalley *et al.*, 1992; Riciputi & Paterson, 1994). However, these technologies are not yet widely available in the scientific community, highlighting the need for alternative methods to determine the isotope signatures of single-phase, multigenerational carbonate cements.

The present investigation quantitatively examines the importance of varying amounts of different siderite cement generations on carbon and oxygen isotope signatures in the Lower Permian Tirrawarra Sandstone of the Moorari and Fly Lake Fields, Cooper basin, South Australia (Fig. 1). The data are based on the integration of petrographic, electron microprobe and fluid inclusion techniques to derive a new procedure for isotope interpretations using back-scattered electron (BSE) image analysis. They show that variations in the isotopic character of siderite cement that generally appears homogeneous under the optical microscope are a function of the relative proportion and composition of each generation of siderite cement, which are best characterized using BSE imaging techniques in the study area.

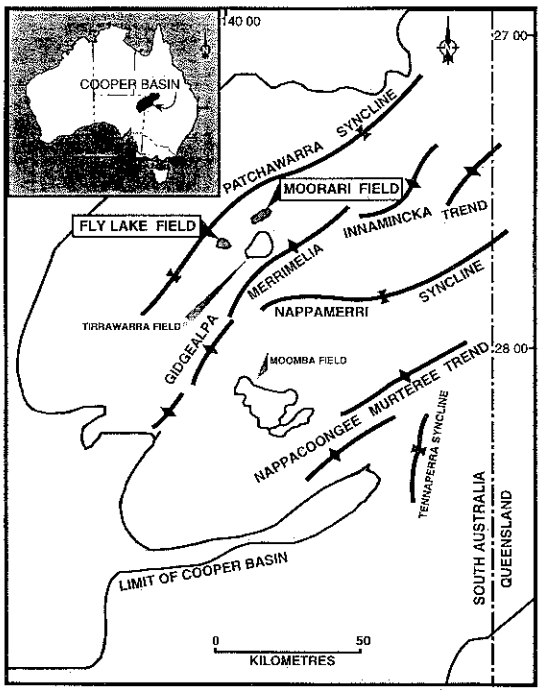

Fig. 1. Map of the southern Cooper basin showing major structural elements and the location of the Moorari and Fly Lake Fields in the Patchawarra syncline, Cooper basin. Modified from Stuart *et al.* (1988).

GEOLOGICAL SETTING

The Permo-Triassic Cooper basin of central Australia (Fig. 1) is Australia's largest onshore hydrocarbon province, containing about 6 TCF of recoverable gas and 300 MMSTB of oil and gas liquids (Heath, 1989; Laws, 1989). The basin consists dominantly of lacustrine–fluvial deposits with local glaciofluvial and rare paraglacial aeolian sediments (see Kapel, 1966, 1972; Gatehouse, 1972; Battersby, 1976; Stuart, 1976; Thornton, 1979; Williams *et al.*, 1985; Fairburn, 1989). The basin is unconformably underlain by the Early Palaeozoic marine and volcanic rocks of the Warburton basin (Gatehouse, 1986) and unconformably overlain by the Jurassic–Cretaceous sediments of the Eromanga basin (Exon & Senior, 1976; Senior *et al.*, 1978; Armstrong & Barr, 1986). Each of these basins has a different areal extent, and the various depocentres shifted over geological time. Cooper basin sediment deposition terminated at the end of the Early–Mid-Triassic, when widespread compressional folding, regional uplift and erosion occurred (Battersby, 1976). Rejuvenation of pre-Permian faults along the flanks of many structures occurred contemporaneously with Cooper basin deposition (Battersby, 1976; Stuart, 1976; Apak *et al.*, 1993). The basin is characterized by three major synclinal areas, namely the Patchawarra, Nappamerri and Tennapperra synclines, which are separated by the Gidgealpa–Merrimelia–Innamincka (GMI) and Murteree–Nappacoongee (MN) anticlinal trends (Fig. 1)

(Thornton, 1979; Apak, 1994). The synclinal areas contain up to 2500 m of Permian sediments, overlain by as much as 1300 m of Jurassic to Tertiary strata (Battersby, 1976; Thornton, 1979). Fluvial sandstones which occur at various levels within the Permian section represent the main petroleum reservoirs, including the fluvioglacial Tirrawarra Sandstone (Smyth, 1979; Kantsler *et al.*, 1983; Heath, 1989; Hunt *et al.*, 1989; Yew & Mills, 1989). About 95% of the Cooper basin oil occurs in the Tirrawarra Sandstone of the Tirrawarra Field (Heath, 1989) (Fig. 2). Additional oil reserves are found at the same stratigraphical interval in the Moorari and Fly Lake Fields (Fig. 1). The two fields were discovered in 1971 and are fault-bounded anticlinal structures. In both, the Tirrawarra Sandstone reservoirs are characterized by relatively low ambient pore porosities (9–12%), low permeabilities (0.1–15 mD *in situ*) and hence relatively low productivities (25–600 BOPD) (Rodda & Paspaliaris, 1989; Yew & Mills, 1989).

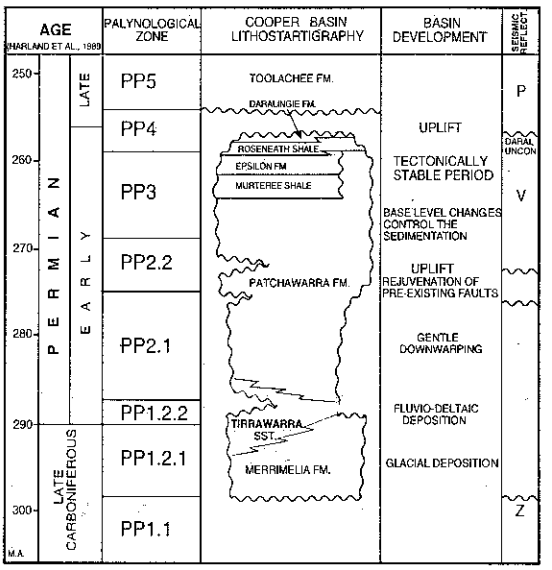

Fig. 2. Stratigraphic column for the southern Cooper basin and main tectonic events. The fluvio-deltaic Tirrawarra Sandstone was deposited during the early subsidence history of the Cooper basin when Australia was at high southern latitudes. Modified from Apak *et al.* (1993), Apak (1994) and Seggie *et al.* (1994).

PREVIOUS INVESTIGATIONS

Many workers have commented on the depositional environment of the Tirrawarra Sandstone. Thornton (1979) suggested deposition in a braided river system, whereas Williams & Wild (1984) and Wild (1987) proposed a low-sinuosity, bed-load dominated fluvial channel origin. Seggie *et al.* (1994) proposed a braid-delta origin for the Tirrawarra Sandstone in the Tirrawarra Field. Limited data are available concerning the regional diagenetic evolution of the Tirrawarra Sandstone. Various authigenic minerals have been identified in Cooper basin sediments, including quartz, carbonates, kaolinite, dickite and illite, and locally clinochlore and pyrophyllite in the central Nappamerri Syncline (Stanley & Halliday, 1984; Schulz-Rojahn & Phillips, 1989; Schulz-Rojahn, 1991; Stuart *et al.*, 1991). Carbonate cement types include siderite, ankerite, dolomite, ferroan dolomite and, rarely, calcite (Stuart *et al.*, 1990; Schulz-Rojahn, 1991). Based on a regional database, Schulz-Rojahn (1991) noted that siderite is about 17 times more abundant by volume than all other carbonate varieties together in the Cooper basin sediments, and a major cause of porosity reduction, including in the Tirrawarra Sandstone. Martin (1981) studied the Tirrawarra Sandstone in six wells of the Tirrawarra Field and interpreted the siderite cement to be an early diagenetic event. Martin (1984) investigated 40 Tirrawarra Sandstone samples in the Tirrawarra, Moorari and Fly Lake Fields, and concluded that the siderite pre-dates quartz cementation. Bever *et al.* (1987, 1988) investigated the Tirrawarra Sandstone in the Tirrawarra and Moorari Fields and also concluded that the siderite is an early cement that possibly provided early structural support against grain compaction.

METHODS

A total of 130 core samples from the Tirrawarra Sandstone were collected from 14 wells of the Moorari and Fly Lake Fields. Sedimentological descriptions of the cores were made and samples from rocks deposited in a variety of depositional environments were collected.

Thin sections were prepared for all samples following impregnation with blue-dyed epoxy resin to facilitate the recognition of porosity. Quantitative estimates of sandstone mineralogy, texture and porosity were obtained by point counting (400–600 counts per thin section).

Semiquantitative bulk-rock XRD analyses were carried out on 46 core samples (Table 1). The samples were gently crushed in ethanol using an agate mortar and pestle, and then dried in an oven at a temperature less than 60°C to minimize clay damage. Randomly oriented powders were prepared by cavity-mounted pressing in an aluminium holder. The prepared samples were run in a Phillips PW 1050 X-ray diffractometer at 50 kV and 35 mA, using Co(K_α) radiation, at a scan speed of 2° per minute. Semiquantitative mineral identification was based on comparison with JCPDS files using the CSIRO software Xplot.

Table 1. Derivation of the Tirrawarra Sandstone core samples. Mineralogical compositions were determined by semiquantitative bulk-rock XRD analysis. Siderite is the only carbonate cement present, but occurs in varying proportions

Well name	Sample no.	Depth (mkB)	Qtz	Kao	I/M	Sid
Fly Lake 1	F1-9397	2864.2	D	M	T	D
Fly Lake 1	F1-9417	2825.1	D	M	T	M
Fly Lake 1	F1-9431	2875.2	D	D	T	S
Fly Lake 2	F2-9554	2912.1	D	T	T	T
Fly Lake 2	F2-9561	2914.2	D	T	T	?
Fly Lake 2	F2-9568	2916.3	D	T	T	T
Fly Lake 2	F2-9570	2916.9	D	S	T	T
Fly Lake 2	F2-9583	2920.9	D	M	T	D
Fly Lake 2	F2-9590	2923.0	D	D	T	S
Fly Lake 2	F2-9598	2924.3	D	S	T	M
Fly Lake 3	F3-9588	2921.5	D	M	T	M
Fly Lake 3	F3-9593	2923.9	D	D	T	T
Fly Lake 4	F4-9441	2877.6	D	T	T	D
Fly Lake 5	F5-9401	2865.4	D	T	T	T
Fly Lake 5	F5-9454	2881.6	D	T	T	–
Fly Lake 6	F6-9398	2864.5	D	T	T	–
Fly Lake 6	F6-9401	2865.4	D	T	T	T
Moorari 1	M1-9420	2872.4	D	T	T	M
Moorari 1	M1-9596	2924.9	D	T	T	T
Moorari 1	M1-9598	2925.5	D	T	T	M
Moorari 1	M1-9613	2930.0	D	D	T	T
Moorari 1	M1-9620	2936.1	D	M	T	S
Moorari 2	M2-10090	3075.4	D	T	T	M
Moorari 2	M2-10116	3083.4	D	T	T	M
Moorari 2	M2-10127	3086.7	D	T	T	T
Moorari 2	M2-10145	3092.2	D	T	T	T
Moorari 3	M3-9422	2868.8	D	T	T	M
Moorari 3	M3-9440	2874.6	D	M	T	T
Moorari 3	M3-9465	2884.9	D	T	T	T
Moorari 3	M3-9465	2885.2	D	M	T	–
Moorari 3	M3-9501	2895.9	D	T	T	T
Moorari 3	M3-9503	2896.5	D	M	T	T
Moorari 4	M4-9507	2897.7	D	T	T	–
Moorari 4	M4-9523	2902.6	D	T	T	–
Moorari 4	M4-9531	2905.0	D	T	T	–
Moorari 4	M4-9554	2912.1	D	M	T	M
Moorari 5	M5-9458	2882.8	D	D	T	T
Moorari 5	M5-9463	2884.3	D	T	T	–
Moorari 5	M5-9510	2898.6	D	M	T	T
Moorari 5	M5-9513	2899.6	D	M	T	T
Moorari 5	M5-9528	2904.1	D	T	T	–
Moorari 5	M5-9583	2874.8	D	T	T	T
Moorari 6	M6-9780	2980.9	D	T	T	T
Moorari 7	M7-9589	2922.7	D	S	T	T
Moorari 9	M9-9732	2966.3	D	M	T	D

Qtz, quartz; Kao, kaolinite; I/M, illite/muscovite; Sid, siderite; D, dominant (peak >1200 counts); S, subdominant (800 <main peak >1200); M, minor (400 <main peak >800); T, trace (peak <400).

SEM studies were carried out on broken rock surfaces and polished sections coated with carbon and gold/palladium using a Phillips XL20 electron microscope connected to a back-scattered electron (BSE) detector. Energy-dispersive X-ray (EDX) analysis was employed to study the composition of representative authigenic minerals.

Determination of quantitative elemental composition of siderite cement was carried out on polished thin sections covered with a thin layer of carbon and using a CAMECA SX 51 electron microprobe at 15 kV, with a 20 nA beam current and a 0.2 μm beam diameter. The BSE imaging system linked to the electron microprobe was used to detect zonation in the siderite cement, and composition analyses were carried out for each zone (Table 2). Results were normalized to 100 mol% Fe + Mn, Mg and Ca. The precision of the analyses was 100% ± 2. The standards used were: MgO for Mg, wollastonite for Ca, rhodonite for Mn, and Fe_2O_3 for Fe.

Oxygen and carbon isotope analyses were carried out on 18 core samples which were selected using optical and bulk XRD methods (Table 3). Only samples containing major amounts of siderite that lack other carbonate cement types (as identified in bulk XRD and under the electron microprobe) were selected for stable isotope analysis. The samples were crushed to a fine dry powder, and then left to react with 100% phosphoric acid under vacuum at 100°C overnight (Rosenbaum & Sheppard, 1986). The resultant carbon dioxide was purified according to conventional techniques (McCrea, 1950) and analysed on a 6-inch dual-collector VG Micromass 602E mass spectrometer. The acid correction factors of Rosenbaum & Sheppard (1986) were used to compensate for the oxygen isotope fractionation. Stable isotope values are reported in the δ notation in parts per thousand (‰). All oxygen isotope ratios are reported relative to standard mean ocean water (SMOW) (Craig, 1961) and all carbon isotope values relative to PDB (Craig, 1957).

Table 2. Microprobe results (mol%) for the different siderite cement generations, which can be further subdivided on the basis of colour variations under the BSE microscope

Well name	Sample no.	FeO (%)	MgO (%)	CaO (%)	MnO (%)	Colour code
Fly Lake 1	F1-9431	60.59	37.09	1.51	0.80	S2d
	F1-9431	67.73	30.85	0.36	1.06	S2m
	F1-9431	80.24	19.03	0.07	0.66	S3l
	F1-9431	71.89	27.41	0.04	0.66	S3m
	F1-9431	68.39	29.65	1.22	0.74	S3d
	F1-9431	77.79	21.32	0.15	0.74	S3m
Fly Lake 2	F2-9570	77.17	21.55	0.51	0.77	S3l
	F2-9583	96.90	0.24	1.16	1.69	S1l
	F2-9583	75.88	22.92	0.20	1.00	S2m
Moorari 1	M1-9613	63.72	34.45	1.03	0.80	S2d
	M1-9613	85.27	11.09	2.00	1.64	S2l
	M1-9613	78.27	19.98	1.05	0.70	S2m
	M1-9620	94.81	1.09	2.50	1.61	S1l
	M1-9620	79.65	19.14	0.34	0.87	S2m
Moorari 2	M2-10116	70.66	27.92	0.46	0.96	S2d
	M2-10116	65.88	32.78	0.26	1.08	S2m
	M2-10116	63.48	34.82	0.48	1.22	S3d
	M2-10116	81.82	16.83	0.35	1.00	S3l
	M2-10116	68.49	29.78	0.56	1.17	S3m
	M2-10145	70.56	28.71	0.12	0.61	S2d
	M2-10145	77.15	20.18	0.96	1.71	S2l
	M2-10145	69.92	28.96	0.31	0.80	S2m
	M2-10145	84.97	9.07	1.57	4.39	S3l
	M2-10145	82.78	15.48	0.73	1.01	S3m
Moorari 3	M3-9422	93.89	2.02	2.83	1.26	S1l
	M3-9422	81.23	14.44	3.58	0.74	S2m
	M3-9440	81.44	17.38	0.25	0.93	S2m
	M3-9440	78.45	20.40	0.23	0.92	S3d
	M3-9440	77.13	21.51	0.41	0.95	S3m
	M3-9503	61.62	37.43	0.27	0.68	S2d
	M3-9503	83.29	13.08	1.32	2.32	S2l
	M3-9503	76.10	22.37	0.40	1.13	S2m
Moorari 4	M4-9574	63.60	35.21	0.08	1.11	S2d
	M4-9574	87.21	10.78	0.14	1.87	S2l
	M4-9574	74.39	23.78	0.49	1.34	S2m
	M4-9574	80.82	17.41	0.42	1.35	S3l
	M4-9574	77.12	20.96	0.31	1.62	S3m
Moorari 5	M5-9553	63.83	34.54	0.26	1.38	S2d
	M5-9553	82.49	14.93	0.37	2.21	S2l
	M5-9553	65.52	32.77	0.21	1.50	S2m
	M5-9553	58.97	39.72	0.14	1.18	3D
	M5-9553	72.84	25.87	0.25	1.04	S3m
	M5-9553	69.46	29.34	0.22	0.98	S3d
Moorari 6	M6-9737	89.03	9.39	0.16	1.42	S3l
	M6-9737	75.07	23.55	0.29	1.08	S3d
	M6-9737	86.32	12.32	0.12	1.23	S3m
Moorari 7	M7-9606	58.36	39.97	0.29	1.38	S2d
	M7-9606	79.67	18.27	1.16	0.89	S2m
Moorari 9	M9-9732	97.05	0.85	0.93	1.18	S1l
	M9-9732	68.05	30.30	1.06	0.59	S2d
	M9-9732	82.82	15.99	0.21	0.98	S2l
	M9-9732	75.20	23.08	0.89	0.83	S2m
	M9-9732	91.11	7.85	0.04	1.00	S3l

l, light-coloured; m, moderately light-coloured; d, dark-coloured in BSE image.

Table 3. Carbon and oxygen isotope data of the Tirrawarra Sandstone siderite cements. A good match is observed between measured ($\delta^{18}O_{meas}$) and calculated oxygen isotope values ($\delta^{18}O_{calc}$), determined from image analysis results. The isotope data reflect the varying proportions of the different generations of siderite cement

Well name	Sample	$\delta^{13}C$ (PDB ‰)	$\delta^{18}O$ (PDB ‰)	$\delta^{18}O_{meas}$ (SMOW ‰)	S1 (%)	S2 (%)	S3 (%)	$\delta^{18}O_{calc}$ (SMOW ‰)	Facies
Moorari 5	M5-9583	−10.37	−23.38	6.6	0	3	97	6.28	BD
Moorari 2	M2-10145	−11.13	−23.83	6.15	0	5	95	6.41	BD
Moorari 4	M4-9574	−10.68	−21.39	8.59	0	40	60	8.58	BS
Moorari 7	M7-9606	−10.49	−22.70	7.28	15	30	55	9.33	BM
Moorari 2	M2-10116	−8.13	−19.12	10.86	10	43	47	9.68	BS
Fly Lake 1	F1-9417	−3.83	−15.80	14.18	19	38	43	10.19	BD
Moorari 6	M6-9737	−9.70	−18.79	11.19	8	51	41	9.99	BS
Fly Lake 1	F1-9431	−4.22	−18.50	11.48	0	60	40	9.82	BD
Moorari 1	M1-9598	−7.07	−17.56	12.42	36	38	26	11.73	BD
Moorari 3	M3-9440	−5.98	−15.37	14.61	80	13	7	14.19	BS
Fly Lake 2	F2-9583	1.45	−15.84	14.14	92	3	5	14.66	MBB
Moorari 3	M3-9503	−7.97	−17.67	12.31	0	98	2	12.18	BD
Moorari 1	M1-9613	−9.22	−18.23	11.75	3	95	2	12.26	BD
Moorari 4	M4-9554	−8.95	−17.17	12.81	5	93	2	12.32	BS
Moorari 9	M9-9732	−4.99	−15.71	14.27	60	39	1	13.98	BM
Moorari 3	M3-9422	−3.87	−14.85	15.13	98	1	1	15.08	BM
Moorari 1	M1-9620	−6.23	−16.70	13.28	15	85	0	12.74	BD
Fly Lake 4	F4-9441	1.46	−16.01	13.97	100	0	0	15.20	MBB

S1, early siderite cement; S2, middle generation siderite cement; S3, late generation siderite cement; BD, distal braid delta; BM, medial braid delta; BS, beach-barrier sandstone; MBB, back-barrier marsh.

Twelve samples were selected for fluid inclusion analysis. Cycling methods (Reynolds, 1978) were employed to carry out microthermometry on small primary fluid inclusions. The fluid inclusion analysis was carried out on a Leitz optical microscope with a warming–cooling Reynolds stage. In all of the siderite samples, isolated fluid inclusions of two-phase liquid–vapour were present. The petrographic features of the fluid inclusions are consistent with a primary origin (see Goldstein & Reynolds, 1994). Because the fluid inclusions were small it was not possible to observe the final melting of the ice. The size of the fluid inclusions, which were mostly equidimensional, suggesting that no stretching has occurred, was between 3 and 6 μm for both the S2 and S3 siderite cement generations. The microthermometry measurement precision is estimated at ±1 °C.

Different generations of siderite cement were identified and characterized using a Phillips image analysis system in conjunction with the SEM. The BSE images of carbon-coated polished thin sections were imported from the SEM in the form of grey-scale binary images (0–256 scale) using a video camera and a Windows-based software program called Image Analysis.

Generally, each main generation of siderite cement was characterized by a distinct range of grey-scale values in any one sample, reflecting varying elemental compositions of the carbonate cement. Quantitative estimation of these different siderite cement generations was accomplished by assigning a unique colour code to the range of grey-scale values representative of each cement generation in each sample. For all samples, the same analytical procedure was followed:

1 Acquisition of the BSE image of siderite cement. Mg-poor (early-formed) siderite cement was found to be relatively light-coloured, whereas more Mg-rich siderite is darker in colour.

2 Adjustment of contrast and brightness of the grey-scale image to enhance visual differentiation of the various cement generations for each field of view.

3 Production of an on-screen histogram showing the frequency distribution of the range of grey-scale values represented in each BSE image, and the selection of grey-scale threshold values representative of each major cement generation for the purpose of colour coding (e.g. red (S1) = 0–80; green (S2) = 81–160; yellow (S3) = 161–256).

4 Computerized colour conversion of the grey-scale BSE image using the manually defined pixel threshold values. In the Tirrawarra Sandstone each major

generation of siderite cement was generally characterized by a unique colour, reflecting different chemical compositions.

5 Automatic determination of the relative abundance of each user-defined colour zone, representing a different cement generation in this study. Machine readings were verified by random visual inspection of some micrographs using a grid overlay, and in all cases the machine results were found to be almost identical to the ones obtained by the human operator. In order to obtain a statistically meaningful set of results, between 20 and 30 fields of view were analysed for each sample (magnification × 100). On average, about 2 minutes were needed to analyse each field of view.

The potential shortcomings of the image analysis technique relate to the fact that BSE images only provide a two-dimensional representation of the rock volume, which may lead to errors in the statistical analysis of cement (colour) abundances. In rare cases, owing to compositional similarities between different generations of siderite cement and the resultant low grey-scale contrast, estimation of the relative abundance of the cement generations could not be carried out. Only samples for which the relative abundance of each generation of siderite cement could be ascertained were integrated with the oxygen and carbon isotope data in this investigation. The image analysis technique cannot be applied in regions where different siderite cement generations have the same chemical composition, or overlapping compositions.

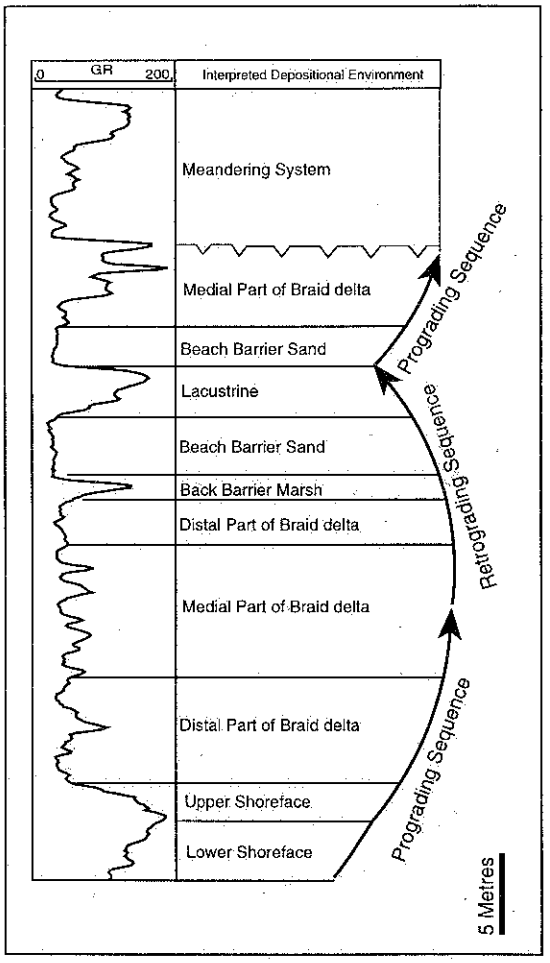

Fig. 3. Example of the different depositional environments and progradational and retrogradational cycles of the Tirrawarra Sandstone in the Moorari and Fly Lake Fields. The gamma ray log trace is derived from the Moorari 9 well.

RESULTS

Palaeoenvironmental interpretations

Various depositional palaeoenvironments are recognized in the Tirrawarra Sandstone (Fig. 3), including lacustrine, parallel beach-barrier, back-barrier marsh with outwash beds, distal and medial braid-delta, meandering system and aeolian depositional environments. The lacustrine deposits include both upper- and lower-shoreface clastics. Parallel beach-barrier sandstones are chiefly medium-grained, well-sorted quartzarenites. Back-barrier marsh sediments consist of massive mudstones, fine-grained sandstones and thin coal beds. The distal braid-delta sediments, which include linguoid bars, interchannel bay and splay deposits, are composed of dominantly medium to coarse-grained, moderately sorted sandstones containing some thin mudstone intercalations. The medial braid-delta clastics include massive and trough cross-bedded conglomerates and pebbly, trough and planar cross-bedded, very coarse-grained, poorly sorted sandstones. The meandering system is composed of matrix-supported oligomictic gravel lag, medium-grained well-sorted point-bar quartzarenites, and floodplain mudstone and coals. The aeolian beds are thin, medium-grained supermature quartzarenites that formed on the point-bar sands during times of low water discharge.

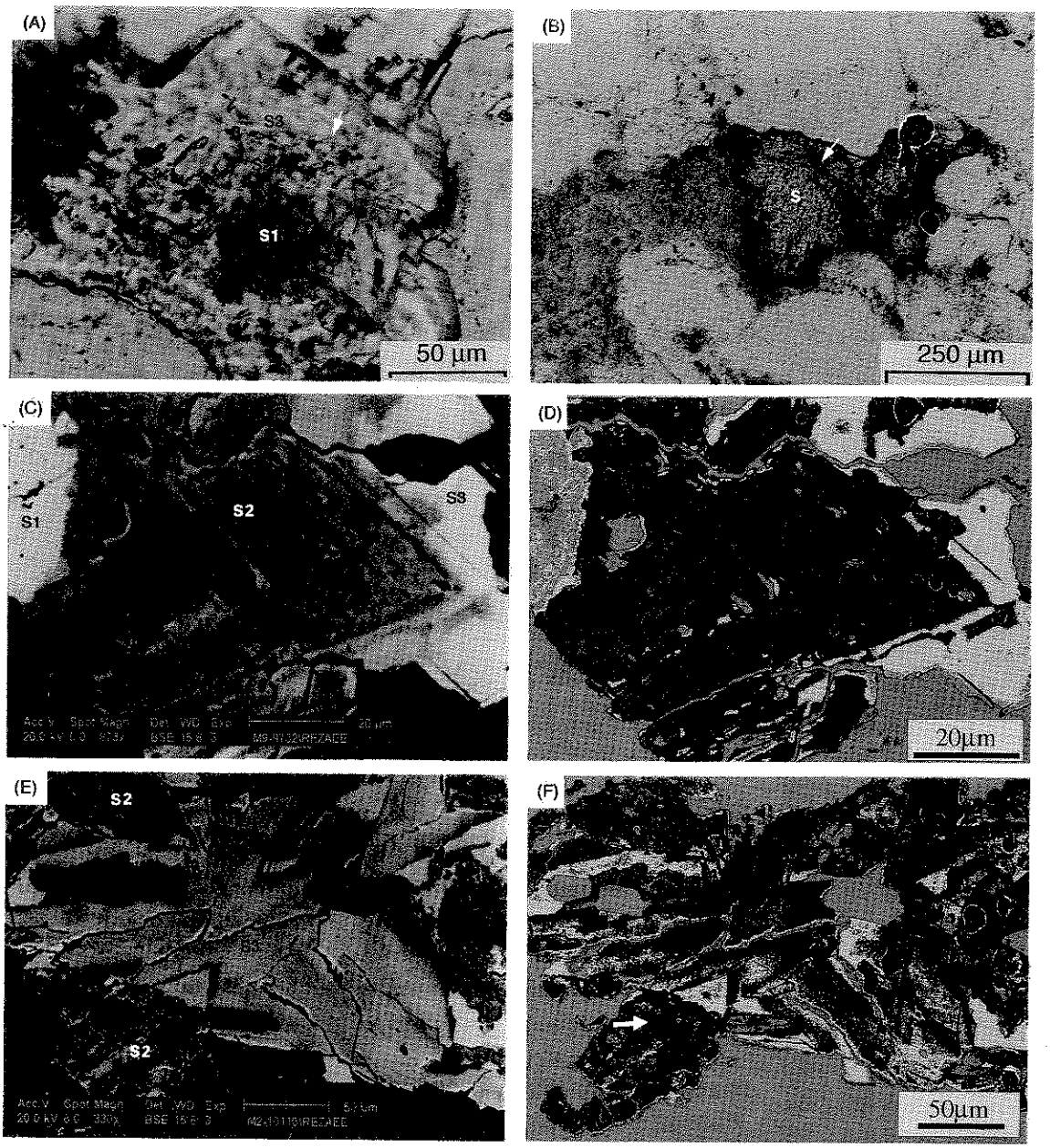

Fig. 4. Petrographic, BSE and colour image characteristics of Tirrawarra Sandstone siderites. (A) Plane-polarized view of the main siderite cement generations that can be distinguished under the optical microscope in this case, which is the exception rather than the rule. S1 has a brownish colour, whereas S2 and S3 are clear and colourless. S1 is typically engulfed by S2. Note the concentration of fluid inclusions in S2, and the irregular serrated boundary between S2 and S3 (arrow), implying some dissolution of S2 prior to precipitation of S3. Sample M1-9598, Moorari 1, 2925.5 m. (B) More typical, homogeneous-looking siderite spar with irregular, serrated edges adjacent to kaolinite booklets (arrow), indicating some siderite dissolution prior to kaolinite precipitation. Sample M3-9503, Moorari 3, 2896.5 m. Plane-polarized view. (C) BSE image illustrating the cement stratigraphy. Light-coloured homogeneous S1,

Continued

General diagenetic characteristics

Tirrawarra Sandstones in the Moorari and Fly Lake Fields consist mainly of medium-grained, moderately sorted sublitharenites (mostly mica schist and phyllite, shale and siltstone clasts) (classification of Folk, 1974). A variety of authigenic minerals are recognized, including syntaxial quartz overgrowths, minor illite, patchy kaolinite and siderite. Attention is focused on the siderite and only a short description of the other diagenetic minerals is provided here.

Quartz is the dominant pore-filling cement in most samples. CL studies show at least six generations of quartz cement, although three main phases are distinguished. The homogenization temperatures of fluid inclusions entrapped within the quartz cement indicate that this precipitated at temperatures between 65 and 130°C, unless the fluid inclusions re-equilibrated during burial (see Osborne & Haszeldine, 1993; Haszeldine & Osborne, 1993). Present-day reservoir temperature is about 124–136°C in the study area. Quartz cementation was initiated prior to major compaction, as evidenced by the loose grain packing of detrital grains, but probably continued until relatively recent times.

Pore-filling euhedral and vermiform kaolinite booklets are common, and are sometimes intergrown with the outer margin of quartz overgrowths. The kaolinite is believed to have formed mainly as a replacement product of feldspars, and to a lesser extent micas.

The authigenic nature of illite is evident from its rare fibrous, lath-like habit. XRD analysis indicates that the mineral is a dioctahedral 2M1 variety with a relatively broad base to the 10 Å peak, indicative of either a poorly crystalline nature or possible interstratification with other minerals. The mineral is thought to have formed as a replacement product of chemically unstable rock fragments.

Siderite cement characteristics

Siderite cement occurs in varying proportions in the Tirrawarra Sandstone and constitutes up to about 30% of rock volume in some samples, as determined by point counting. It is the only carbonate cement present in the samples (Table 1). Siderite generally occurs as isolated sparry rhombs or as a pore-filling cement, although a variety of different crystal habits are apparent, including rhombohedral, blocky and radial forms. The bulk-rock XRD traces provide no clues to the presence of multiple siderite cement generations. Rarely is the presence of different generations of siderite cement evident under the petrographic microscope (Fig. 4A). However, when viewed under the electron microprobe and using the BSE imaging technique, three main generations of siderite cement are identified, including early (S1), middle (S2) and late (S3) (Figs 4C–F and 5–8). The proportion of each generation quantified by BSE image analysis varies from sample to sample (Table 3). Fluid inclusion data indicate that the different generations precipitated under different temperature conditions. Integration of the BSE image analysis data with bulk-rock siderite isotope results suggests that both oxygen and carbon isotope characteristics are controlled by the relative abundance of each cement generation.

Early generation of siderite cement (S1)

Under the optical microscope, S1 has a blotchy appearance, displays a moderately light to dark brown colour (Fig. 4A) and appears devoid of fluid inclusions. In some samples S1 is the only siderite

Fig. 4. (*Continued*) characterized by an irregular outer edge, is engulfed by S2 displaying broad, uneven compositional zoning, which in turn is surrounded by S3. Sample M9-9732, Moorari 9, 2966.3 m. (D) Colour-enhanced BSE image of the same view as shown in (C) (see text). The method helps to differentiate the main generations of siderite cement. Although the settings need to be adjusted from sample to sample, each main generation of siderite cement tends to be characterized by a unique range of colours, which facilitates volumetric estimation of the relative proportions of S1, S2 and S3 in each sample. Some compositional variation is evident in S1, the dissolution boundary between S1 and S2 is more enhanced, and the boundary between S2 and S3 can clearly be seen to be very sharp and irregular in nature. Note the homogeneous texture of S3. (E) BSE image showing S2, which has a variably dark-grey colour and fringes the edges of a pore that was subsequently filled by a very homogeneous, light-grey S3 cement. S2 is of a pseudorhombic nature. Sample M2-10116, Moorari 2, 3083.4 m. (F) The same view as shown in (E), colour enhanced. The micrograph illustrates problems with the image analysis technique in some samples. Whereas S2 and S3 can clearly be differentiated in most areas of the view shown, S2 locally displays a mixture of both colours (arrow), rendering volumetric estimation of the different cement generations difficult in this sample. This problem is the exception rather than the rule in the Tirrawarra Sandstones.

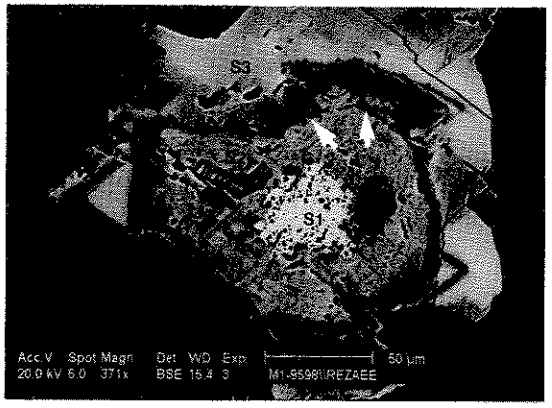

Fig. 5. BSE image of the view shown in Fig. 4(A). S1 displays a light colour, whereas the surrounding S2 (medium grey) is characterized by a variable internal composition and complex zoning. S3 is a relatively homogeneous, late-generation pore-filling cement. Note the irregular dissolution boundary between S1 and S2, and between S2 and S3 (arrows). These cement relationships are typical of Tirrawarra Sandstones. Sample M1-9598, Moorari 1, 2925.5 m.

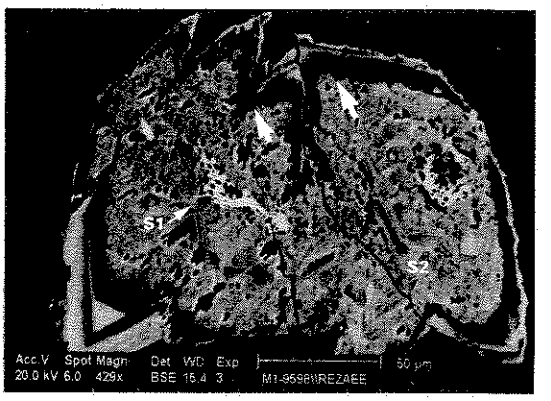

Fig. 7. In this BSE image S1 occurs as isolated patchy white remnants (arrow) within S2 cement (medium grey), which is characterized by an inhomogeneous appearance and complex zoning. S2 is enclosed by a relatively homogeneous, euhedral S3 cement displaying some broad compositional zoning. Note the presence of dissolution pits in S2 and the characteristic dissolution boundary (arrows) between S2 and S3. Sample M1-9598, Moorari 1, 2925.5 m.

cement, especially in fine-grained poorly sorted marsh sediments rich in organic matter. In samples where S1 cements the rock completely, quartz grains are characterized by a very loose grain packing (high intergranular volume), with individual grains apparently 'floating' in the siderite matrix (Fig. 9). Where other siderite cement generations are present, S1 generally represents the substrate or nucleus for the middle generation of siderite cement precipitation (S2) (Figs 5–8). The boundary between S1 and S2 is not always distinct, but is typically characterized by irregular and serrated

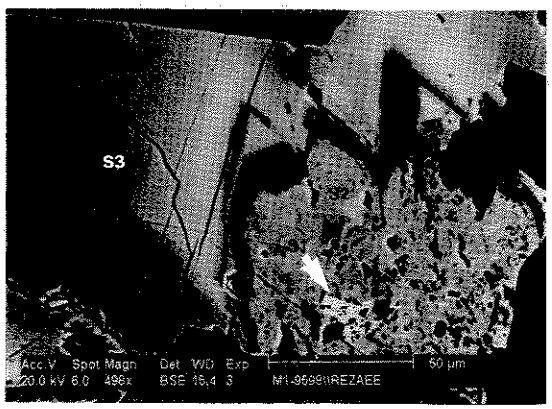

Fig. 6. In this BSE image a homogeneous S3 cement is the main pore-filling event; however, examination of other micrographs shows that the relative proportion of the different siderite cement generations can vary with different fields of view (*cf.* Figs 4A and 5). Again, notice the dissolution boundary between S2 and S3, the dissolution pits associated with S2, and the isolated remnants of S1 (arrow) within the S2 matrix. Further observe the incipient euhedral rhombic terminations of the S3 cement that grew on the S2 dissolution surface. Sample M1-9598, Moorari 1, 2925.5 m.

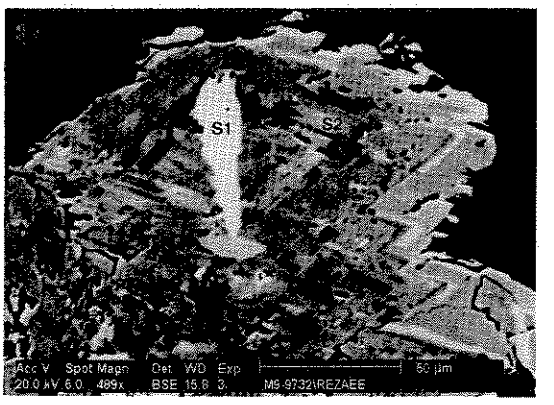

Fig. 8. BSE image showing remnant S1 cement with dissolution edges (white) engulfed by abundant S2 cement (dark grey) that displays complex compositional variation. Sample M9-9732, Moorari 9, 2966.3 m.

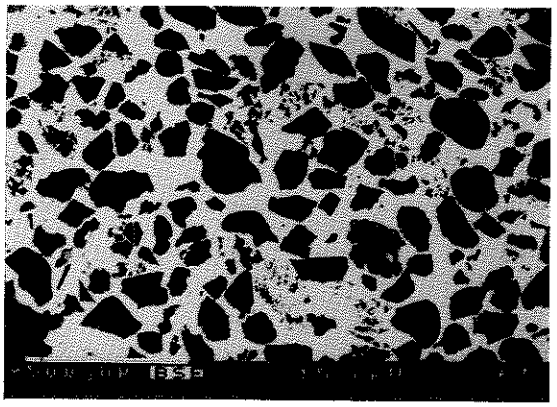

Fig. 9. BSE image of a fine-grained, moderate to poorly sorted back-barrier marsh sample completely cemented by S1 (white). Note the serrated nature of some quartz grains and the very high intergranular volume (>50%), which suggest the replacement of part of the margins of quartz grains by siderite cement. Sample F4-9441, Fly Lake 4, 2877.6 m. Scale bar = 500 μm.

edges, indicating some dissolution of S1 prior to S2 cementation (Fig. 5). In the BSE image S1 is light coloured and appears homogeneous (Figs 5–9). Electron microprobe analysis for S1 shows a high Fe/Mg ratio (Fig. 10). The S1 elemental composition ranges from $(Fe_{97.7\%}Mg_{0.8\%}Ca_{0.7\%}Mn_{0.8\%})CO_3$ to $(Fe_{93.4\%}Mg_{2\%}Ca_{3.3\%}Mn_{1.3\%})CO_3$, with the average composition being $(Fe_{96\%}Mg_{1\%}Ca_{1.7\%}Mn_{1.3\%})CO_3$. In samples dominated by S1 (92–98%), oxygen isotope compositions range from +14.1‰ to +15.1‰, with $\delta^{13}C$ compositions varying between −3.8 and +1.45‰. The one sample in which S1 constitutes 100% of the siderite cement volume (sample F4-9441) has a $\delta^{18}O$ value of +13.97‰ and a $\delta^{13}C$ of +1.46‰ (Table 3).

Middle generation of siderite cement (S2)

In BSE images S2 has the appearance of rhombs, which generally enclose S1 nuclei (Figs 5–8) and which in turn are engulfed by S3. Differentiation between S2 and S3 is difficult under the optical microscope, except where small dissolution pits and boundaries occur between S2 and S3 (Fig. 4A). S2 is characterized by many small (3–5 μm) primary fluid inclusions, whereas S3 has fewer inclusions. Locally, S2 is engulfed by quartz cement, indicating that quartz cementation postdates S2 precipitation (Fig. 11). In BSE image S2 displays a multiple compositional zoning (Fig. 12).

Based on grey-scale characteristics, three main zones of S2 precipitation are evident, namely dark-, medium- and light-coloured zones. Electron microprobe analysis reveals different elemental compositions and variable substitution of Mg for each of the S2 subgenerations (Tables 2 and 5). S2 compositions range from $(Fe_{87.2\%}Mg_{9.5\%}Ca_{0.7\%}Mn_{2.6\%})CO_3$ to $(Fe_{56.7\%}Mg_{42.2\%}Ca_{0.15\%}Mn_{0.95\%})CO_3$, with the average composition being $(Fe_{74\%}Mg_{24\%}Ca_{0.8\%}Mn_{1.2\%})CO_3$ (Table 4), representing sideroplesite for the light-coloured zone and pistomsite for the medium- to dark-coloured zone (classification of Deer *et al.*, 1992). In samples in which S2 is the dominant carbonate cement phase (93–98%), oxygen isotope values range from +12.3‰ to +12.8‰ and carbon isotope values between −9.2‰ and

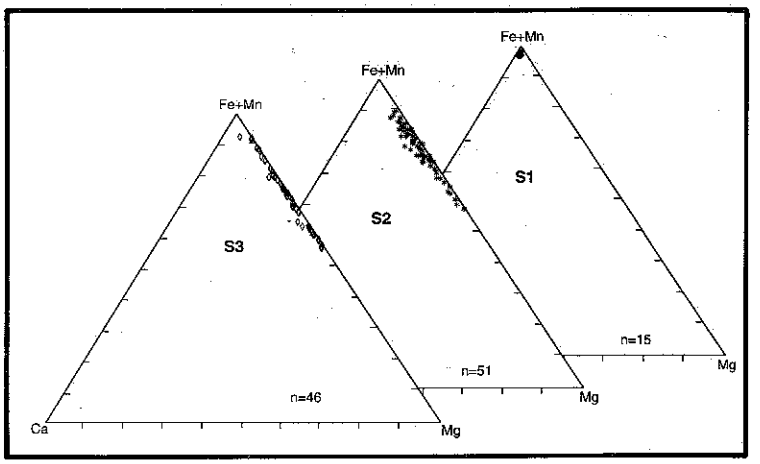

Fig. 10. Ternary diagrams showing the compositional ranges of different generations of siderite cement in the Tirrawarra Sandstone. The early generation of the siderite cement (S1) is very rich in Fe, whereas the middle (S2) and late generations (S3) have much higher substitution of Mg and fall within the realm of sideroplesite and pistomsite. S2 and S3 have almost identical compositions except that S2 has a slightly higher Ca content.

Fig. 11. BSE image showing the intergrowth between S2 cement (white) displaying characteristic rhombs and quartz overgrowths (medium grey). Locally the siderite is completely engulfed by the quartz cement (arrow), indicating that some siderite cementation preceded quartz (Q) cementation. Sample F1-9433, Fly Lake 1, 2875.2 m. Scale bar = 50 μm.

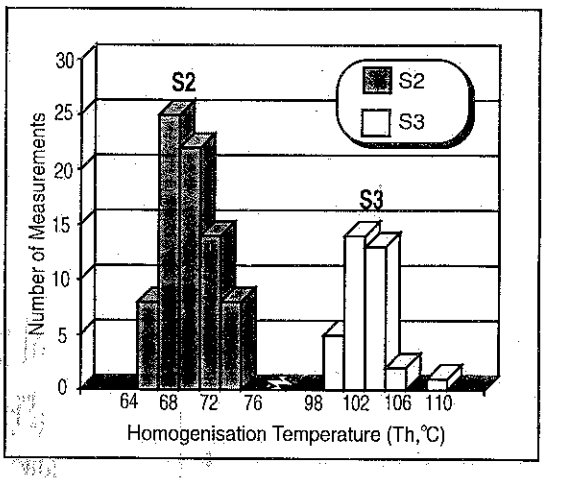

Fig. 13. Fluid inclusion homogenization temperatures for the middle (S2) and late generations (S3) of the Tirrawarra Sandstone siderites. The fluid inclusions are considered to be of primary origin, and did not experience stretching. S2 formed at much lower temperatures than S3.

−7.9‰. The mean $\delta^{13}C$ composition is about −8.6‰, and the average $\delta^{18}O$ composition is +12‰ for S2 (Table 4). Homogenization temperatures of S2 fluid inclusions range from 66 to 76°C, with a median of around 68°C (Fig. 13).

Late generation of siderite cement (S3)

Under the optical microscope S3 is a blocky, colourless, very clear cement (Fig. 4a), postdating S1 and S2. The boundary between S2 and S3 is characterized by an irregular serrated outline, implying some dissolution of S2 prior to precipitation of S3 (Fig. 14). In some samples oil occurs in the boundary zone between S2 and S3, indicating that hydrocarbon migration occurred synchronous with or after the dissolution event, but prior to S3 precipitation. BSE images show that S3 is a relatively homogeneous cement generation (compared with S2), characterized by an initial high Mg content (pistomsite) grading into a relatively thick, homogeneous sideroplesite cement (Figs 5–7). Electron microprobe analyses indicate extensive substitution of Mg, with an average composition of ($Fe_{75.5\%}$

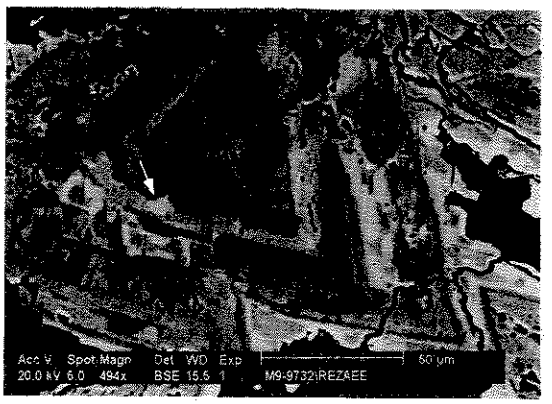

Fig. 12. BSE image of the middle generation of siderite cement (S2), showing compositional zoning and some dissolution. Sample M9-9732, Moorari 9, 2966.3 m.

Table 4. Summary table showing the average isotopic, chemical composition and fluid inclusion characteristics of the main siderite cement generations (S1, S2, S3)

	S1	S2	S3
$\delta^{18}O$ (‰ SMOW)	+15	+12	+6
$\delta^{13}C$ (‰ PDB)	+1.45	−8.5	−11
T_h (°C)	–	68	102
FeO (%)	96	74	75.5
MgO (%)	1.0	24	23
CaO (%)	1.7	0.8	0.5
MnO (%)	1.3	1.2	1.0

T_h, fluid inclusion homogenization temperature.

Table 5. Average elemental composition (mol%) of different zones within the main siderite cement generations (S1, S2, S3). Subdivisions of the main siderite cement generations are based on colour differences under the BSE microscope

	S1l	S2l	S2m	S2d	S3l	S3m	S3d
FeO (%)	95.7	83.0	74.7	64.6	83.6	76.8	69.0
MgO (%)	1.0	14.3	23.6	34.0	14.4	21.8	29.6
CaO (%)	1.9	0.8	0.7	0.6	0.4	0.3	0.4
MnO (%)	1.4	1.8	1.0	0.9	1.5	1.1	1.0

l, light-coloured; m, moderately light-coloured; d, dark-coloured in BSE image.

$Mg_{23\%}Ca_{0.5\%}Mn_{1\%})CO_3$ for S3 (Table 4). In samples which contain the highest proportion of S3 (95–97%) oxygen isotope compositions range from +6.1‰ to +6.6‰, with $\delta^{13}C$ compositions varying between −11.1‰ and −10.4‰. For these samples mean oxygen and carbon isotope values are about +6‰ and −11‰, respectively (Table 4). Fluid inclusion results for S3 indicate a homogenization temperature of between 98 and 114°C, with a median of about 102°C (Fig. 13).

Bulk $\delta^{18}O$ and $\delta^{13}C$ trends

A broad correlation exists between $\delta^{18}O$ and $\delta^{13}C$ values for the different samples containing multiple siderite cement generations (Fig. 15). With increasing enrichment in $\delta^{18}O$, $\delta^{13}C$ values become less negative. The isotope results of the samples dominated by a single siderite cement generation plot within narrow zones, whereas the ones derived from samples with varying proportions of the different cement generations plot between these zones in a broad scatter (Fig. 15). Samples deposited under marsh environments are characterized by relatively high $\delta^{13}C$ and $\delta^{18}O$ values, reflecting the dominance of S1 in these sediments. In contrast, siderites that formed in rocks deposited under different sedimentary conditions have generally more ^{13}C- and ^{18}O-depleted isotope signatures owing to the greater proportion of S2 and S3 in these samples (Table 3).

Fig. 14. Scanning electron micrograph showing euhedral, blocky siderite thought to represent the S3 cement generation that developed on an earlier, partly dissolved siderite cement surface (S2). Sample M3-9405, Moorari 3, 2847.8 m.

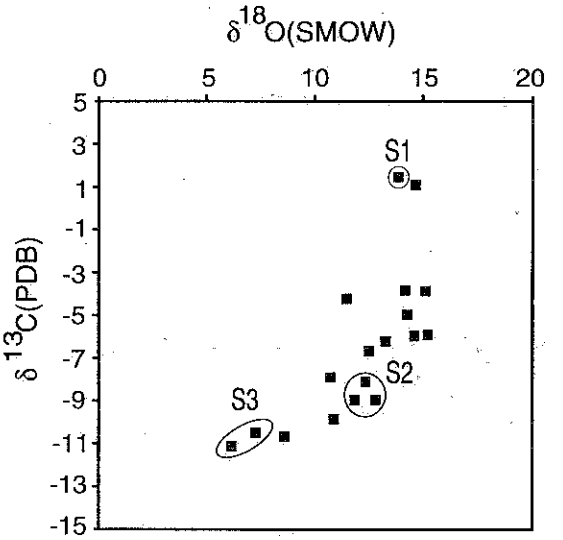

Fig. 15. Cross-plot of carbon and oxygen isotope values for the Tirrawarra Sandstone siderites. The bulk-rock isotope signatures are the cumulative product of the varying proportions of the different siderite cement generations (S1, S2, S3). The pure end-member compositions of the different siderite cement generations can be estimated from samples which are dominated by a single cement generation (circled areas). Only the end-member isotope compositions of the different cement generations should be taken into consideration when evaluating multigeneration siderite cements.

DISCUSSION

The integration of bulk-rock isotope data with electron microprobe and image analysis results has led to the identification of a multigeneration pore-filling siderite cement in the Tirrawarra Sandstone of the Moorari and Fly Lake Fields. Although previous workers had identified several siderite cement morphologies, they had assumed the pore-filling sparry siderite to be a single-generation precipitate in Cooper basin sediments (Martin & Hamilton, 1981; Schulz-Rojahn & Phillips, 1989).

Results from the present investigation show that the pore-filling siderite precipitated in three main stages in the Moorari–Fly Lake area. An early, homogeneous Fe-rich siderite (S1) was followed by a generally more extensive cement generation characterized by a complex compositional zoning (S2). This in turn was engulfed by a late-generation, relatively homogeneous (compared with S2) siderite cement (S3). The relative proportion of each cement generation varies between samples, and in some rocks one or two of these siderite cement generations are absent (Table 3). The identification of multiple siderite cement generations is of importance for the interpretation of bulk-rock oxygen and carbon isotope results in the Cooper basin, and probably also in other geological provinces.

In the Tirrawarra Sandstone each generation of siderite cement has a distinct isotope signature, as revealed by samples which are dominated by a single cement generation ($\geq$ 95%). Only a small proportion of the samples fall into this category (Table 3). The majority of the isotope results are the cumulative product of the varying proportions of the different siderite cement generations. Failure to recognize this fact may lead to erroneous interpretations of the isotope data. For example, the broad trend of overall more negative $\delta^{13}C$ values with increasing depletion in ^{18}O (Fig. 15) could be interpreted as a continuous (gradual) evolution in carbonate isotope composition during burial diagenesis. The trend is commonly observed in carbonate cements in a variety of clastic provinces (Fritz *et al.*, 1971; Irwin *et al.*, 1977; Irwin, 1980; Schulz-Rojahn, 1991; Mozley & Carothers, 1992; Spötl *et al.*, 1993). However, results from the present investigation show that the pattern can also be produced by sample heterogeneity. The data demonstrate that major changes in pore fluid isotope composition occurred between the precipitation of each major cement generation in the Tirrawarra Sandstone (Fig. 15). The conclusion is supported by the presence of a dissolution boundary between each major cement generation (Figs 4A and 5).

Further, non-recognition of the isotopically heterogeneous nature of most Tirrawarra Sandstone samples could lead to erroneous perceptions of the major source(s) of carbon for siderite precipitation. In the study area, a high proportion of $\delta^{13}C$ values for the siderites fall within the range of about −3 and −8‰ (Fig. 15). Without a knowledge of the influence of differential cement development on bulk-rock isotope signatures, the values could be attributed mainly to mixing of carbon derived from marine limestones (+2 to −2‰; Hudson, 1977) and volcanic or geothermal sources (on average between −5 and −7‰; Deines, 1986). However, as the isotope values within the range of −3 and −8‰ are derived from samples that contain multiple siderite cement generations in varying proportions (Table 3), these hybrid data provide no useful clues to the conditions under which the different generations formed.

The approach differs from other investigations of diagenesis, in which there is no discrimination of the bulk-rock isotope data and where all bulk-rock isotope values are used to derive a model of carbonate cementation. Difficulties in estimating the volume of individual cement generations generally prohibit a greater qualitative control on isotope interpretations. However, the present study shows that BSE image analysis can provide an efficient means of quantifying the influence of multigenerational cement development on bulk-rock isotope signatures, if it is assumed that BSE-derived cement generations are isotopically homogeneous.

Method for enhanced isotope interpretation

In the study area the influence of variable cement proportions on $\delta^{18}O$ can be determined by plotting the relative abundances of S1, S2 and S3 for each sample on a ternary diagram (Fig. 16a). The samples with the highest proportion of a single cement generation give the closest approximation to end-member $\delta^{18}O$ values, and provide the basis for the labelling of each corner of the diagram. IsoSMOW lines can then be drawn which allow the prediction of $\delta^{18}O$ values for the remainder of the samples (Fig. 16b). In cases where there is no end-member representative, the IsoSMOW lines established from existing values can be extrapolated to the end-member locations at the corners of the ternary

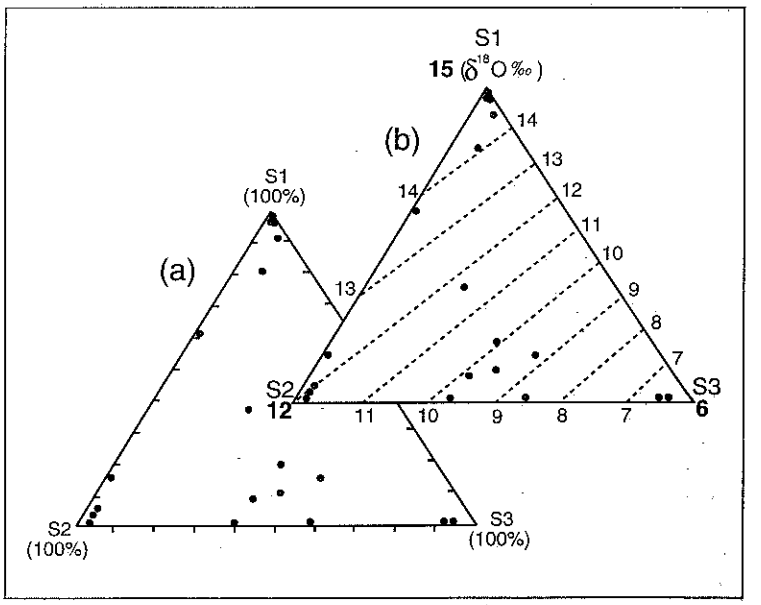

Fig. 16. (a) Ternary diagram showing the relative abundance (%) of the different siderite cement generations in the Tirrawarra Sandstone, as determined from statistical evaluation of electron microprobe and image analysis results. (b) The samples with the highest proportion of a single cement generation give the closest approximation to end-member $\delta^{18}O$ values (+15‰, +12‰ and +6‰ were assumed for 100% pure S1, S2 and S3 respectively, based on the data shown in Table 3). IsoSMOW lines can then be constructed for the remainder of the samples. The application of the method is the calculation of isotope compositions for individual siderite cement generations in samples which contain more than one siderite cement generation.

diagram, in order to estimate end-member $\delta^{18}O$ values. The relationship can be expressed by the equation

$$\delta^{18}O_{(bulk)} = (V_{S1} \times \delta^{18}O_{S1}) + (V_{S2} \times \delta^{18}O_{S2}) + (V_{S3} \times \delta^{18}O_{S3})$$

where $\delta^{18}O_{(bulk)}$ is the oxygen isotope result of the bulk-rock analysis; V_{S1} is the proportion of S1; V_{S2} is the proportion of S2; V_{S3} is the proportion of S3; $\delta^{18}O_{S1}$ is the oxygen isotope value of S1; $\delta^{18}O_{S2}$ is the oxygen isotope value of S2; and $\delta^{18}O_{S3}$ is oxygen isotope value of S3.

Table 3 shows that the measured and calculated bulk-rock $\delta^{18}O$ values generally exhibit a good correlation ($r^2 = 0.82$). Minor discrepancies between the two data sets are probably due to small errors in the estimation of the volume of individual cement generations in some samples. The bulk-rock $\delta^{13}C$ composition of each sample is also controlled by the relative proportion of each generation of siderite cement, and the same mathematical formula as shown above (substituting $\delta^{13}C$ for $\delta^{18}O$) can be applied. However, the correlation coefficient for calculated $\delta^{13}C$ values ($r^2 = 0.64$) is lower than the one for calculated $\delta^{18}O$ compositions. We are uncertain about the reason(s) for this phenomenon, but believe it may be due to the fact that $\delta^{18}O$ in a cement, at any given pore-water isotope composition, is a strongly temperature-dependent variable, whereas $\delta^{13}C$ is independent of temperature.

Both $\delta^{18}O$ and $\delta^{13}C$ values for each end-member cement generation plot within narrow zones (Fig. 15), allowing a precise definition of the conditions under which the individual cement generations formed, albeit based on a small data set. The data show that the quantitative approach to isotope analysis provides added precision to routine bulk-rock isotope interpretation methods in the study area. The technique used in this study may be applicable to other geological provinces, provided different cement generations do not have the same chemical composition. The image analysis technique is particularly valuable for rocks in which pure or nearly pure samples of carbonate cement end-members do not exist.

Precipitation temperatures of siderite cement

In the study area compositional zoning is evident in both the S2 (Figs 8 and 12) and S3 (Fig. 6) cement generations, indicating that the cements precipitated from solution and did not undergo recrystallization during burial diagenesis. No unstable precursor for siderite is known, and there is no documented case of siderite recrystallization (Mozley & Carothers, 1992). For these reasons, fluid inclusions are thought to provide a genuine record of the temperatures at which the Tirrawarra Sand-

stone siderites crystallized, unless resetting of the inclusions (McLimans, 1987; Prezbindowski & Larese, 1987; Prezbindowski & Tapp, 1991) did occur. However, consistent differences in homogenization temperatures between S2 and S3 (Fig. 13) suggest that the fluid inclusions did not undergo re-equilibration, in view of the fact that appreciable differences in the size of the fluid inclusions were not detected between S2 and S3. Further, present temperatures at reservoir level exceed the maximum homogenization temperatures of S3 by at least 20–30°C, indicating that the fluid inclusions did not reset during recent geological times. Geohistory modelling shows that Cooper basin sediments did not undergo major subsidence in the last few million years in the Patchawarra syncline (Tupper & Burckhardt, 1990). Therefore, we conclude that S2 precipitated at a mean water temperature of about 68°C, whereas S3 formed at about 102°C on average (Fig. 13).

No fluid inclusion data are available for S1; however, the cement stratigraphy would suggest that S1 crystallized at temperatures lower than those for S2, i.e. less than about 68°C. During the Early Permian the palaeolatitude of central Australia was about 70–75° south (McElhinny, 1969; Embleton & McElhinny, 1982; Veevers, 1984). The $\delta^{18}O$ of recent meteoric water is between −15 and −16‰ at this latitude (Dansgaard, 1964). Accordingly, if we assume a $\delta^{18}O$ value of −15.5‰ for Early Permian pore water, then S1 must have precipitated at a temperature of about 30°C, which does indeed correspond to relatively early diagenesis.

Sources of carbon

In the Tirrawarra Sandstone, carbon isotope values show that major changes in conditions occurred between the precipitation of S1 and the later siderite cement generations, S2 and S3. Whereas the sample where S1 is the only siderite cement present has a $\delta^{13}C$ composition of about +1.45‰, those samples dominated by S2 or S3 are much more depleted in ^{13}C (Fig. 15).

The $\delta^{13}C$ character of S1 is consistent with a major source of carbon involving methanogenesis (Curtis & Coleman, 1986). Although a marine source of carbon (−2 to +2‰; Hudson, 1977) could also theoretically explain the observed $\delta^{13}C$ composition of S1, this explanation is inconsistent with the fluvio-lacustrine nature of the Cooper basin sediments. Locally, marine Warburton basin limestones of Cambrian to Early Ordovician age unconformably underlie the Cooper basin sediments (Battersby, 1976; Gatehouse, 1986). However, it is most unlikely that any mineral components were derived from this limestone source during S1 precipitation, because there is an almost complete absence of calcite cement in the Cooper basin. The minor calcite cement that is present in Permian sediments tends to concentrate in the shallowest Cooper basin sediments, furthest away from the Warburton Basin limestones (Schulz-Rojahn, 1991). Further, it is unclear why upwelling fluid movement from these limestones should have coincided with S1 precipitation but not S2 and S3 precipitation, and how this very late fluid movement could have been accomplished in view of the fact that more than 180 million years separate the deposition of the Cambro-Ordovician limestones and the Tirrawarra Sandstone. Therefore, a major source of carbon involving methanogenesis is the most probable explanation for the $\delta^{13}C$ character of S1.

During methanogenesis, strongly ^{13}C-depleted methane and ^{13}C-enriched carbon dioxide is produced by microbial activity (Rosenfeld & Silverman, 1959; Hudson, 1977). Acetate fermentation is the most likely cause of methanogenesis in fresh-water depositional environments (Whiticar *et al.*, 1986). In modern marsh sequences, highly ^{13}C-enriched values are produced by methanogenic processes during early diagenesis (Moore *et al.*, 1992). The carbonate cements produced from bacterial fermentation reactions start to precipitate at some depth below the sediment–water interface ($\leq$10 m) from pore waters supersaturated with ^{13}C-rich bicarbonate ($\leq$ +15‰), and the $\delta^{13}C$ composition of the pore water becomes progressively poorer in ^{13}C with increasing burial depth ($\geq$1000 m) (Irwin *et al.*, 1977). In the present study the concentration of S1 in marsh sediments, coupled with the petrographic evidence and the fact that the elemental composition of S1 is similar to that described by Mozley (1989) for early fresh-water siderite cement in different geological provinces, suggests that this cement generation formed in the relatively shallow diagenetic realm. However, S1 probably precipitated below the initial zone of pore water supersaturated with ^{13}C-rich bicarbonate as described by Irwin *et al.* (1977), because S1 has a $\delta^{13}C$ composition of +1.45‰ rather than +15‰.

Preferential removal of ^{12}C by organic materials (Schidlowski *et al.*, 1975, 1976; Faure, 1986) can also contribute toward the ^{13}C enrichment of sider-

ite in organic-rich marsh sediments. In the Tirrawarra Sandstone, both this process and methanogenesis probably produced the positive $\delta^{13}C$ character of the S1 cement.

The later siderite cement generations (S2 and S3) are relatively closely related in terms of their carbon isotope signatures, having $\delta^{13}C$ values of −8.5 and −11‰, respectively (Fig. 15). They also have extensive substitution by Mg, which was probably derived from the alteration of Mg-rich minerals (such as micas), which are abundant in nearly all of the Tirrawarra Sandstones, including in metamorphic rock fragments. This source of Mg was suggested by Macaulay *et al.* (1993) for siderite cements in the Magnus Sandstone, North Sea. Mg could also have been released from kerogen after burial (Desborough, 1978). According to Desborough (1978), the higher content of magnesium with respect to calcium in kerogen-rich rocks is probably due to the preferential concentration of magnesium by blue–green algae, whose remains released magnesium during kerogen maturation. The $\delta^{13}C$ compositions of both S2 and S3 are consistent with a major source of carbon involving the thermal decarboxylation of organic matter, which produces a strongly ^{12}C-enriched carbon (see Hudson, 1977; Irwin *et al.*, 1977; Carothers & Kharaka, 1980; Kharaka *et al.*, 1983). The same source of carbon was proposed by Morad *et al.* (1994) for Mg-rich siderites in fluvial Triassic sandstones from southern Tunisia.

Significance of dissolution events

The results from this investigation show that siderite can undergo repeated cycles of precipitation and dissolution during the diagenetic history of a basin, and that secondary porosity which is produced as a result of siderite leaching can be a temporary phenomenon in clastic provinces. Because it cannot be determined how much siderite cement was dissolved during each dissolution event, it is uncertain whether the secondary porosity was volumetrically significant in the past. However, the rather subtle nature of the dissolution boundaries would suggest relatively minor dissolution events. The dissolution boundaries almost certainly mark a substantial time gap between the precipitation of each major generation of siderite cement, as is indicated by the different isotope compositions and the fluid inclusion data of the various cement generations.

The first dissolution event (D1) occurred between the precipitation of S1 and S2, at reservoir temperatures probably between about ≤30 and 68°C, as suggested by the stable isotope and fluid inclusion data. The second dissolution phase (D2) took place after the formation of S2 but before S3 cementation, in the temperature range of about 68–102°C (Fig. 17).

The origin of the dissolution events is uncertain, but in the case of D1 may be related to the invasion of low-pH meteoric pore waters during kaolinite precipitation (see Bjørlykke & Brendsdal, 1986). The presence of oil at the dissolution boundary between S2 and S3 may point to the role of organic processes in triggering carbonate cement dissolution, prior to or synchronous with petroleum migration. The second dissolution phase (D2) broadly coincides with the temperature window for peak hydrocarbon generation (see Tissot & Welte, 1978). It is possible that organic acids which accompanied kerogen maturation (Schmidt & McDonald, 1979; Surdam *et al.*, 1984; Burley, 1986) triggered the dissolution event. According to Curtis (1983), maturing kerogen can generate Al-bearing acidic pore water that produces late-generation kaolinite. In the

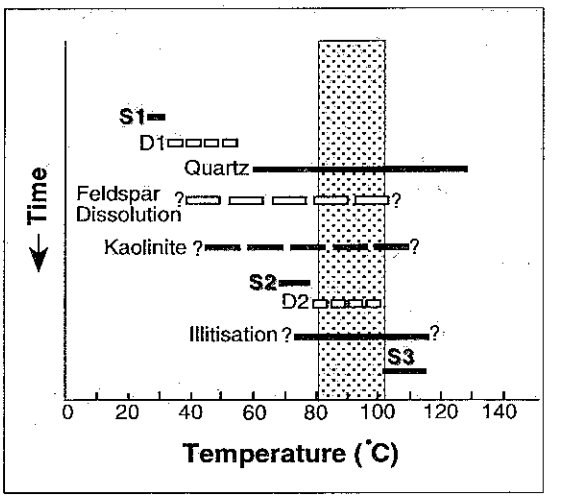

Fig. 17. Generalized paragenetic sequence for the Tirrawarra Sandstone in the Fly Lake–Moorari area, Cooper basin. The interpretation is based on the integration of petrographic, isotope and fluid inclusions results. The estimated timing of oil generation and migration is indicated (shaded zone). S1, early generation of siderite cement; S2, middle generation of siderite cement; S3, late generation of siderite cement; D1 and D2, first and second phases of siderite dissolution, respectively.

Tirrawarra Sandstone, either meteoric invasion or source-rock maturation probably accounts for the association of authigenic kaolinite patches with siderite spar displaying dissolution (Fig. 4B).

CONCLUSIONS

Multigenerational siderite in the Tirrawarra Sandstone of the Moorari and Fly Lake Fields highlights the important role of differential cement development on bulk-rock isotope signatures. The results from this investigation show that caution must be exercised in the interpretation of bulk-rock isotope signatures, even when only a single carbonate cement phase is indicated by semiquantitative bulk XRD analysis. Failure to recognize isotopically heterogeneous samples may lead to erroneous interpretations of the isotope results. Only the end-member isotope compositions of the different cement generations should be taken into consideration when interpreting the genesis of multigeneration siderite cements. Generally, the different generations are not readily identifiable under the optical microscope, highlighting the importance of BSE image analysis for siderite characterization. In particular, the integrated use of video capture and image analysis software provides an efficient means of quantifying the different siderite cement generations seen under BSE. As the method can be semi-automated, the technique provides a potentially powerful tool for improved bulk-rock isotope interpretations in clastics containing multigenerational carbonate cements. It allows the determination of end-member $\delta^{18}O$ and $\delta^{13}C$ compositions of individual cement generations in cases where pure, or nearly pure, samples of end-member carbonate cement generations are not available for isotope analysis, provided that a statistically representative number of BSE images is analysed, and that the various cement generations have different chemical compositions.

In the Tirrawarra Sandstone of the Moorari and Fly Lake Fields, the application of the BSE image analysis technique, together with bulk-rock isotope and fluid inclusion studies, has led to the identification of three main generations of siderite cement. The first and second generations were each followed by at least one dissolution event. The first generation of siderite cement is a homogeneous Fe-rich siderite with a $\delta^{13}C$ signature of +1.45‰, which probably formed during low-temperature methanogenesis (≤30°C). The second generation is an Mg-rich inhomogeneous siderite characterized by a complex zoning, with a $\delta^{13}C$ signature of −8.5‰. It is thought to have formed mainly by the decarboxylation of organic matter at temperatures between 64 and 76°C. The third and final precipitation event produced an Mg-rich, relatively homogeneous pore-filling siderite with a $\delta^{13}C$ character of −11‰. This is also interpreted to have formed during kerogen maturation, albeit at more elevated temperatures (98–110°C). The results from this study show that organic processes controlled siderite cementation over a range of different burial conditions in the study area.

ACKNOWLEDGEMENTS

The authors thank Drs Nick Lemon (NCPGG) and John Collen (Victoria University of Wellington) for their constructive criticisms of the draft manuscript. The manuscript was greatly improved by the comments of IAS reviewers Drs Sadoon Morad (University of Uppsala), Earle F. McBride (University of Texas at Austin) and Richard Worden (Queen's University of Belfast). The authors gratefully acknowledge the financial support of the NCPGG, the Australian Research Council (ARC) and SANTOS Ltd.

REFERENCES

Al-Aasm, I.S., Taylor, B.E. & South, B. (1990) Stable isotope analysis of multiple carbonate samples using selective acid extraction. *Chem. Geol.*, **80**, 119–125.

Apak, S.N. (1994) *Structural development and control on stratigraphy and sedimentation in the Cooper Basin Australia.* PhD thesis, University of Adelaide, 105 pp.

Apak, S.N., Stuart, W.J. & Lemon, N.M. (1993) Structural–stratigraphic development of the Gidgealpa–Merrimelia–Innamincka Trend with implications for petroleum trap styles, Cooper Basin, Australia. *Aust. Petrol. Explor. Ass. J.*, **33**, 94–104.

Armstrong, J.D. & Barr, T.M. (1986) The Eromanga Basin. An overview of exploration and potential. In: *Eromanga Basin Symposium* (Eds Moore, P.S. & Mount, T.J.). Geol. Soc. Aust. Spec. Publ., **12**, 25–38.

Bahrig, B. (1989) Stable isotope composition of siderite as an indicator of the paleoenvironmental history of oil shale lakes. *Palaeogeog., Palaeoclimatol., Palaeoecol.*, **70**, 139–151.

Battersby, D.G. (1976) Cooper Basin oil and gas fields. In: *Economic Geology of Australia and New Guinea*, 3 (Eds Leslie, R.B., Evans, H.J. & Knight, C.L.). Petrol. Australasia Inst. Mineral. Metal., 7, 321–370.

BEVER, J.M. CARROL, P.G., WILLIAMS, B.P.J. & WILD, E.K. (1987) *Petrography and core study, Tirrawarra Sandstone, Moorari and Tirrawarra Fields*, 2 vols. Unpublished report, SAGASCO Ltd, 138 pp.

BEVER, J.M., CARROLL, P.G., WILD, E. & WILLIAMS, B.P.J. (1988) Core facies, petrology, and permeability of Tirrawarra Sandstone, Moorari Field, Cooper Basin, South Australia (abstract). *Bull. Am. Ass. Petrol. Geol.*, **72**, 162.

BJØRLYKKE, K. & BRENDSDAL, A. (1986) Diagenesis of the Brent Sandstone in the Statfjord Field. In: Spec. Publ. Soc. Econ. Paleont. Miner., Tulsa, **38**, 157–167.

BURLEY, S.D. (1986) The development and destruction of porosity within Upper Jurassic reservoir sandstones of the Piper and Tartan Fields, Outer Moray Firth, North Sea. *Clay Mineral.*, **21**, 649–694.

CAROTHERS, W.W. & KHARAKA, Y.K. (1980) Stable carbon isotopes of HCO_3 in oil-field waters—implications for the origin of CO_2. *Geochim. Cosmochim. Acta*, **44**, 323–332.

CARPENTER, S.J., ERICKSON, J.M., LOHMANN, K.C. & OWEN, M.R. (1988) Diagenesis of fossiliferous concretions from the Upper Cretaceous Fox Hills Formation, North Dakota. *J. sediment. Petrol.*, **58**, 706–723.

CRAIG, H. (1957) Isotope standards for carbon and oxygen and correction factors for mass spectrometric analysis of carbon dioxide. *Geochim. Cosmochim. Acta*, **12**, 133–149.

CRAIG, H. (1961) Standards for reporting concentrations of deuterium and oxygen-18 in natural waters. *Science*, **133**, 1833–1834.

CURTIS, C.D. (1983) Link between aluminium mobility and destruction of porosity. *Bull. Am. Ass. Petrol. Geol.*, **63**, 380–384.

CURTIS, C.D. & COLEMAN, M.L. (1986) Controls on the precipitation of early diagenetic calcite, dolomite, and siderite concretions in complex depositional sequences. In: *Roles of Organic Matter in Sediment Diagenesis* (Ed. Gautier, D. L.). Spec. Publ. Soc. Econ. Paleont. Miner., Tulsa, **38**, 23–33.

CURTIS, C.D., PEARSON, M.J. & SOMOGYI, V.A. (1975) Mineralogy, chemistry, and origin of a concretionary siderite sheet (clay–ironstone band) in the Westphalian of Yorkshire. *Miner. Mag.*, **40**, 385–393.

DANSGAARD, W. (1964) Stable isotopes in precipitation. *Tellus*, **16**, 436–468.

DEER, W.A., HOWIE, R.A. & ZUSSMAN, J. (1992) *An Introduction to the Rock-Forming Minerals*. Longman, Harlow, 695 pp.

DEINES, P. (1986) The isotopic composition of reduced organic carbon. In: *Handbook of Environmental Isotope Geochemistry* (Eds Fritz, P. & Fontes, J.Ch.), pp. 329–406. Elsevier Scientific, New York.

DESBOROUGH, G.A. (1978) A biogenic–chemical stratified lake model for the origin of oil shale of the Green River Formation: an alternative to the playa-lake model. *Geol. Soc. Am. Bull.*, **89**, 961–971.

DICKSON, J.A.D., SMALLEY, P.C., RAHEIM, A. & STIJFHOORN, D.E. (1990) Intercrystalline carbon and oxygen isotope variations in calcite revealed by laser microsampling. *Geology*, **18**, 809–811.

EMBLETON, B.J.J. & MCELHINNY, M.W. (1982) Marine magnetic anomalies, palaeomagnetism and the drift history of Gondwanaland. *Earth Planet. Sci. Lett.*, **58**, 141–150.

EXON, N.F. & SENIOR, B.R. (1976) The Cretaceous of the Eromanga and Surat Basins. *Bur. Miner. Resour. J. Aust. Geol. Geophys.*, **1**, 33–50.

FAIRBURN, W.A. (1989) The geometry of Toolachee unit 'C' fluvial sand trends, Moomba Field, Permian Cooper Basin, South Australia. *Aust. Petrol. Explor. Ass. J.*, **29**, 239–250.

FAURE, G. (1986) *Principles of Isotope Geology*, 2nd edn. John Wiley & Sons, Chichester, 589 pp.

FOLK, R.L. (1974) *Petrology of Sedimentary Rocks*. Hemphill, Austin, TX, 182 pp.

FRITZ, P., BINDA, P.L., FOLINSBEE, F.E. & KROUSE, H.R. (1971) Isotopic composition of diagenetic siderites from Cretaceous sediments in Western Canada. *J. sediment. Petrol.*, **41**, 282–288.

GATEHOUSE, C.G. (1972) Formations of the Gidgealpa Group in the Cooper Basin. *Aust. Oil Gas J.*, **18**, 10–15.

GATEHOUSE, C.G. (1986) The geology of the Warburton Basin in South Australia. *Aust. J. Earth Sci.*, **33**, 161–180.

GAUTIER, D.L. (1982) Siderite concretions: indicators of early diagenesis in the Gammon Shale (Cretaceous). *J. sediment. Petrol.*, **52**, 859–871.

GOLDSTEIN, R.H. & REYNOLDS, T.J. (1994) *Systematics of Fluid Inclusions in Diagenetic Minerals*. Soc. Econ. Paleont. Miner. Short Course, **31**, 199 pp.

GOULD, K.W. & SMITH, J.W. (1979) The genesis and isotopic composition of carbonates associated with some Permian Australia coals. *Chem. Geol.*, **24**, 137–150.

HASZELDINE, R.S. & OSBORNE, M. (1993) Fluid inclusion temperatures in diagenetic quartz reset by burial: implications for oil field cementation. In: *Diagenesis and Basin Development* (Eds Horbury, A.D. & Robinson, A.G.). Am. Ass. Petrol. Geol. Studies in Geology, **36**, 35–46.

HEATH, R. (1989) Exploration in the Cooper Basin. *Aust. Petrol. Explor. Ass. J.*, **29**, 366–378.

HUDSON, J.D. (1977) Stable isotopes and limestone lithification. *J. Geol. Soc. London*, **133**, 637–660.

HUNT, J.W., HEATH, R.S. & MCKENZIE, P.F. (1989) Thermal maturity and other geological controls on the distribution and composition of Cooper Basin hydrocarbons. In: *The Cooper and Eromanga Basins, Australia* (Ed. O'Neil, B.J.), pp. 509–523. *Proceedings of the Cooper and Eromanga Basins Conference, Adelaide, 26–27 June 1989*. Petroleum Exploration Society of Australia, Society of Petroleum Engineers, Australian Society of Exploration Geophysicists (SA branches).

IRWIN, H. (1980) Early diagenetic carbonate precipitation and pore fluid migration in the Kimmeridge Clay of Dorset, England. *Sedimentology*, **27**, 577–591.

IRWIN, H., CURTIS, C.D. & COLEMAN, M. (1977) Isotopic evidence for source of diagenetic carbonates formed during burial of organic-rich sediments. *Nature*, **269**, 209–213.

KANTSLER, A.J., PRUDENCE, T.J.C., COOK, A.C. & ZWIGULIS, M. (1983) Hydrocarbon habitat of the Cooper/Eromanga Basin. *Aust. Petrol. Explor. Ass. J.*, **23**, 373–389.

KAPEL, A.J. (1966) The Cooper's Creek Basin. *Aust. Petrol. Explor. Ass. J.*, **6**, 71–75.

KAPEL, A.J. (1972) The geology of the Patchawarra area Cooper Basin. *Aust. Petrol. Explor. Ass. J.*, **12**, 53-57.

KHARAKA, Y.K., CAROTHERS, W.W. & ROSENBAUER, R.J. (1983) Thermal decarboxylation of acetic acid: implications for origin of natural gas. *Geochim. Cosmochim. Acta*, **47**, 397–402.

LAWS, R.A. (1989) Preface. In: *The Cooper and Eromanga Basins, Australia* (Ed. O'Neil, B.J.), pp. v–vi. *Proceedings of the Cooper and Eromanga Basins Conference, Adelaide, 26–27 June 1989.* Petroleum Exploration Society of Australia, Society of Petroleum Engineers, Australian Society of Exploration Geophysicists (SA branches).

MACAULAY, C.I., HASZELDINE, R.S. & FALLICK, A.E. (1993) Distribution, chemistry, isotopic composition and origin of diagenetic carbonates: Magnus Sandstone, North Sea. *J. sediment. Petrol.*, **63**, 33–43.

MARTIN, K.R. (1981) *Petrology and Diagenesis of the Tirrawarra Sandstone in Tirrawarra Field.* Unpublished report, Santos Ltd, 17 pp.

MARTIN, K.R. (1984) *Petrology and Diagenesis and Reservoir Quality of the Tirrawarra Sandstone in Tirrawarra Fly Lake and Moorari Fields.* Unpublished report, Santos Ltd, 31 pp.

MARTIN, K.R. & HAMILTON, N.J. (1981) Diagenesis and reservoir quality, Toolachee Formation, Cooper Basin. *Aust. Petrol. Explor. Ass. J.*, **21**, 143–154.

MATSUMOTO, R. & IIJIMA, A. (1981) Origin and diagenetic evolution of Ca–Mg–Fe carbonates in some coalfields of Japan. *Sedimentology*, **18**, 239–259.

MCCREA, J.M. (1950) On the isotopic chemistry of carbonates and a palaeotemperature scale. *J. Chem. Phys.*, **18**, 849–857.

MCELHINNY, M.W. (1969) The palaeomagnetism of the Permian of southeast Australia and its significance regarding the problem of intercontinental correlation. In: Geol. Soc. Aust. Spec. Publ., **2**, 61–67.

MCLIMANS, R.K. (1987) The application of fluid inclusions to migration of oil and diagenesis in petroleum reservoirs. *Appl. Geochem.*, **2**, 585–603.

MOORE, S.E., FERRELL, R.E. & AHARON, P. (1992) Diagenetic siderite and other ferroan carbonates in a modern subsiding marsh sequence. *J. sediment. Petrol.*, **62**, 357–366.

MORAD, S., BEN ISMAIL, H.N., DE ROS, L.F., AL-AASM, I.S. & SERRHINI, N.-E. (1994) Diagenesis and formation water chemistry of Triassic reservoir sandstones from southern Tunisia. *Sedimentology*, **41**, 1253–1272.

MOZLEY, P.S. (1989) Relation between depositional environment and the elemental composition of early diagenetic siderite. *Geology*, **17**, 704–706.

MOZLEY, P.S. & CAROTHERS, W.W. (1992) Elemental and isotopic composition of siderite in the Kuparuk Formation, Alaska: effect of microbial activity and water/sediment interaction on early pore-water chemistry. *J. sediment. Petrol.*, **62**, 681–692.

OSBORNE, M. & HASZELDINE, R.S. (1993) Evidence for resetting of fluid inclusion temperatures from quartz cements in oilfields. *Mar. Petrol. Geol.*, **10**, 271–278.

PEARSON, M.J. (1985) Some chemical aspects of diagenetic concretions from the Westphalian of Yorkshire, England. *Chem. Geol.*, **31**, 225–244.

PREZBINDOWSKI, D.R. & LARESE, R.E. (1987) Experimental stretching of fluid inclusions in calcite—implications for diagenetic studies. *Geology*, **15**, 333–336.

PREZBINDOWSKI, D.R. & TAPP, J.B. (1991) Dynamics of fluid inclusion alteration in sedimentary rocks: a review and discussion. *Org. Geochem.*, **17**, 131–142.

REYNOLDS, T.J. (1978) *Fluid Inclusion Adapted USGS Gas Flow Heating/Freezing Instruction Manual.* Fluid Incorporated, Denver, CO.

RICIPUTI, L.R. & PATERSON, B.A. (1994) High spatial-resolution measurement of O isotope ratios in silicates and carbonates by ion microprobe. *Am. Mineral.*, **79**, 1227–1230.

RODDA, J.S. & PASPALIARIS, T.G. (1989) Tirrawarra and Moorari Oil Fields enhanced oil recovery schemes—further developments. *Aust. Petrol. Explor. Ass. J.*, **29**, 121–130.

ROSENBAUM, J. & SHEPPARD, S.M.F. (1986) An isotopic study of siderites, dolomites and ankerites at high temperatures. *Geochim. Cosmochim. Acta*, **50**, 1147–1150.

ROSENFELD, W.D. & SILVERMAN, S.R. (1959) Carbon isotope fractionation in bacterial production of methane. *Science*, **130**, 1658–1659.

SCHIDLOWSKI, M., EICHMANN, R. & JUNGE, C. (1975) Precambrian sedimentary carbonates: carbon and oxygen isotope geochemistry and implication for the terrestrial oxygen budget. *Precambrian Res.*, **2**, 1–69.

SCHIDLOWSKI, M., EICHMANN, R. & JUNGE, C. (1976) Carbon isotope geochemistry of the Precambrian Lomagundi carbonate province, Rhodesia. *Geochim. Cosmochim. Acta*, **40**, 449–455.

SCHMIDT, V. & MCDONALD, D.A. (1979) The role of secondary porosity in the course of sandstone diagenesis. In: *Aspects of Diagenesis* (Eds Scholle, P.A. & Schluger, P.R.). Spec. Publ. Soc. Econ. Paleont. Miner., Tulsa, **26**, 175–207.

SCHULZ-ROJAHN, J.P. (1991) *Origin, evolution and controls of Permian reservoir sandstones in the southern Cooper Basin, South Australia.* PhD thesis, National Centre for Petroleum Geology and Geophysics, University of Adelaide, 187 pp.

SCHULZ-ROJAHN, J.P. & PHILLIPS, S.E. (1989) Diagenetic alteration of Permian reservoir sandstones in the Nappamerri Trough and adjacent areas, southern Cooper Basin. In: *The Cooper and Eromanga Basins, Australia* (Ed. O'Neil, B.J.), pp. 629–645. *Proceedings of the Cooper and Eromanga Basins Conference, Adelaide, 26–27 June 1989.* Petroleum Exploration Society of Australia, Society of Petroleum Engineers, Australian Society of Exploration Geophysicists (SA branches).

SEGGIE, R.J., LANSOM, P.B., HAMLIN, H.S. & JOHNSON, G.A. (1994) The Tirrawarra oil field: field revitalisation through reservoir description and characterisation. *Aust. Petrol. Explor. Ass. J.*, **34**, 33–54.

SENIOR, B.R., MOND, A. & HARRISON, P.L. (1978) Geology of the Eromanga Basin. *Bur. Miner. Resour. Bull.*, **167**, 102.

SMALLEY, P.C., MAILE, C.N., COLEMAN, M.L. & ROUSE, J.E. (1992) Lassie (laser ablation sampler for stable isotope extraction) applied to carbonate minerals. *Chem. Geol.*, **101**, 43–52.

SMYTH, M. (1979) Hydrocarbon generation in the Fly Lake–Brolga area of the Cooper Basin. *Aust. Petrol. Explor. Ass. J.*, **19**, 108–114.

SPIRO, B., GIBSON, P.J. & SHAW, H.F. (1993) Eogenetic siderite in lacustrine oil shales from Queensland, Australia, a stable isotope. *Chem. Geol.*, **106**, 415–427.

SPÖTL, C., MATTER, A. & BREVART, O. (1993) Diagenesis and pore water evolution in the Keuper Reservoir, Paris Basin (France). *J. sediment. Petrol.*, **63**, 909–928.

STANLEY, D.J. & HALLIDAY, G. (1984) Massive hydraulic fracture stimulation of Early Permian gas reservoirs, Big Lake Field, Cooper Basin. *Aust. Petrol. Explor. Ass. J.*, **24**, 180–195.

STUART, W.J. (1976) The genesis of Permian and Lower Triassic reservoir sandstones during phases of southern Cooper Basin development. *Aust. Petrol. Explor. Ass. J.*, **16**, 37–47.

STUART, W.J., KENNEDY, S. & THOMAS, A.D. (1988) Influence of structural growth and other factors on the configuration of fluviatile sandstones, Permian Cooper Basin. *Aust. Petrol. Explor. Ass. J.*, **28**, 255–265.

STUART, W.J., FARROW, B.B., LEMON, N.L. & PHILLIPS, S.E. (1990) *Porosity and Permeability in Permian Sandstones: Southern Cooper Basin.* Interim report, NERDDC Project No. 1175, National Centre for Petroleum Geology and Geophysics, University of Adelaide, 104 pp.

STUART, W.J., FARROW, B.B., TINGATE, P.R. *et al.* (1991) *Porosity and Permeability in Permian Sandstones: Southern Cooper Basin.* End-of-grant report, NERDDC Project No. 1407, National Centre for Petroleum Geology and Geophysics, University of Adelaide, 198 pp.

SURDAM, R.C., BOESE, S.W. & CROSSEY, L.J. (1984) The chemistry of secondary porosity. In: *Clastic Diagenesis* (Eds McDonald, D.A. & Surdam, R.C.). Mem. Am. Ass. Petrol. Geol., Tulsa, **37**, 127–149.

THORNTON, R.C.N. (1979) Regional stratigraphic analysis of the Gidgealpa Group, Southern Cooper Basin, Australia. *Geol. Surv. South Aust. Bull.*, **49**, 140 pp.

TISSOT, B.P. & WELTE, D.H. (1978) *Petroleum Formation and Occurrence—a New Approach to Oil and Gas Exploration.* Springer-Verlag, Berlin, 538 pp.

TUPPER, N.P. & BURCKHARDT, D.M. (1990) Use of the methylphenanthrene index to characterise expulsion of Copper and Eromanga Basin oils. *Aust. Petrol. Explor. Ass. J.*, **30**, 373–385.

VEEVERS, J.J. (1984) *Phanerozoic Earth History of Australia.* Oxford Geological Science Series, Oxford University Press, New York, 418 pp.

WHITICAR, M.J., FABER, E. & SCHOELL, M. (1986) Biogenic methane formation in marine and fresh water environments: CO_2 reduction vs. acetate fermentation–isotope evidence. *Geochim. Cosmochim. Acta*, **50**, 693–709.

WILD, E.K. (1987) *The sedimentology and reservoir quality of the Kinnerton Sandstone Formation, UK, and the Tirrawarra Sandstone, S. Australia.* PhD thesis, Department of Geology, University of Bristol.

WILLIAMS, B.P.J. & WILD, E.K. (1984) The Tirrawarra Sandstone and Merrimelia Formation of the Southern Cooper Basin, South Australia—the sedimentation and evolution of a glaciofluvial system. *Aust. Petrol. Explor. Ass. J.*, **24**, 377–392.

WILLIAMS, B.P.J., WILD, E.K. & SUTTILL, R.J. (1985) Paraglacial aeolianites: potential new hydrocarbon reservoirs, Gidgealpa Group, southern Cooper Basin. *Aust. Petrol. Explor. Ass. J.*, **25**, 291–310.

YEW, C.C. & MILLS, A.A. (1989) The occurrence and search for Permian oil in the Cooper Basin, Australia. In: *The Cooper and Eromanga Basins, Australia* (Ed. O'Neil, B.J.), pp. 339–359. *Proceedings of the Cooper and Eromanga Basins Conference, Adelaide, 26–27 June 1989.* Petroleum Exploration Society of Australia, Society of Petroleum Engineers, Australian Society of Exploration Geophysicists (SA branches).